

A Brittle Damage Model: Implementation into LS-DYNA and Application to Normal Plate-on-Plate Impact

Martin N. Raftenberg
U.S. Army Research Laboratory
Aberdeen Proving Ground, MD 21005-5069

Abstract

A brittle damage model developed by M. A. Grinfeld was implemented in the LS-DYNA finite element code and applied to the simulation of normal plate-on-plate impact. The model introduces a state variable measure of damage that evolves in proportion to the elastic strain energy. The model degrades the elastic shear modulus in proportion to the state variable's current level. The implementation procedure by means of the LS-DYNA user-material interface is described. In a simulation of normal plate-on-plate impact, the model produced a gradient in elastic properties within the initially homogeneous target, and this gradient led to a partial reflection of the unloading wave. For a range of values for the material constants introduced by the damage model, the target's free-surface velocity showed a gradual increase over time following the arrival of the initial compressive shock. This observation is discussed in light of the phenomenon of failure waves.

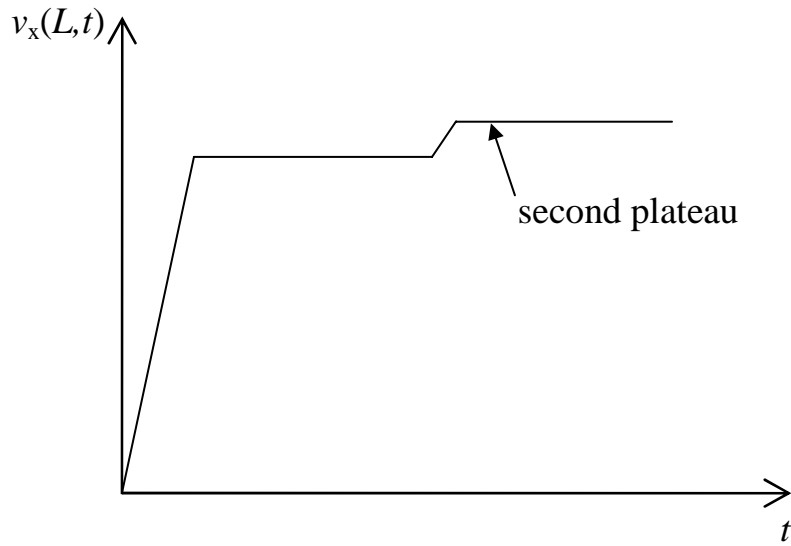
Introduction

Kanel et al. [1] shock-loaded K-19 glass in a normal plate-on-plate impact test, and the VISAR measurement of normal velocity at the free surface contained a second plateau that they interpreted as evidence of a failure wave (Fig. 1a). Impact by the flyer plate introduces a compressive shock into the target plate. This compressive shock traverses the target plate and reaches the free surface, there producing an unloading wave that travels back towards the impacted surface. The hypothesis of Kanel et al. was that, in K-19 glass, before reaching the impacted surface the unloading wave encountered a slower-moving failure front (Fig. 1b). The abrupt change in shock impedance at the failure front caused a partial reflection of the unloading wave. The reflected wave, upon reaching the free surface, produced a second plateau in the velocity signal.

To produce this hypothesized phenomenon in a simulation, a damage model should contain two features. First, the damage evolution equation should introduce one or more time scales, thereby allowing the damage front to lag the initial compressive shock. Second, the shock impedance should be substantially altered from its pre-damaged level.

A particular damage model that contains these features was developed by M. A. Grinfeld and presented in [3, 4]. The next three sections sequentially describe the Grinfeld damage model, its implementation into LS-DYNA [5], and its application to simulations of normal plate-on-plate impact. These are followed by a conclusions section.

(a)



(b)

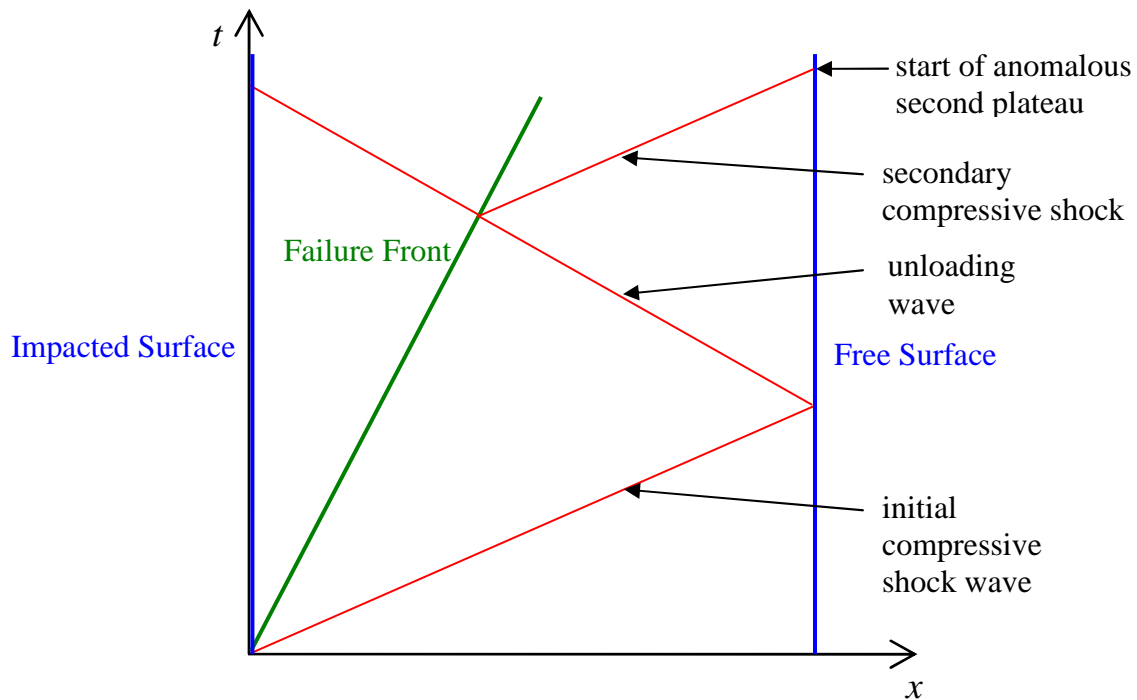


Figure 1. Empirical evidence for failure waves in glass. (a) Sketch of the VISAR signal from the rear surface of a K-19 glass target plate (after Figure 1c in [1]). (b) The hypothesized $x-t$ diagram for the target plate (after Figure 5 in [2]).

The Damage Model

Pre-damaged Material

The model is applied to a material that in its pre-damaged state is isotropic and linearly elastic. Such a pre-damaged material is characterized by an elastic shear modulus, μ , Poisson ratio, ν , and density, ρ . The material's strain energy per unit volume, W_0 , is related to the Green strain tensor, \mathbf{E} , by

$$W_0(E) = \mu \left(\frac{\nu}{1-2\nu} E_{ii} E_{jj} + E_{ij} E_{ij} \right) \quad (1)$$

in which the summation convention on repeated indices applies. In Cartesian coordinates, the components of \mathbf{E} are related to those of the displacement vector, \mathbf{u} , and material position vector, \mathbf{X} , by

$$E_{ij} = \frac{1}{2} \left(\frac{\partial u_i}{\partial X_j} + \frac{\partial u_j}{\partial X_i} + \frac{\partial u_k}{\partial X_i} \frac{\partial u_k}{\partial X_j} \right) \quad (2)$$

Components of the second Piola-Green stress tensor, \mathbf{S} , are related to W_0 by

$$S_{ij} = \frac{\partial W_0}{\partial E_{ij}} \quad (3)$$

Combination of equations 1 and 3 yields

$$S_{ij} = 2\mu \left(\frac{\nu}{1-2\nu} E_{kk} \delta_{ij} + E_{ij} \right) \quad (4)$$

δ_{ij} is the Kronecker delta function, and the summation convention on repeated indices applies.

Damage Evolution

The Grinfeld model introduces damage effects by means of an internal state variable, D , that is a function of position and time. This variable is initialized to zero throughout the material. Thereafter, D monotonically increases according to the evolution equation

$$\dot{D} = -C \frac{\partial \psi}{\partial D} \quad (5)$$

Here, ψ is the Helmholtz free energy per unit volume and C is a material constant with dimensions of time \times distance/mass.

Degradation Function

Degradation function $\phi(D)$ is used to decrease the material's stiffness as damage accrues. $\phi(D)$ relates the Helmholtz free energy density of the damaged material to the elastic strain energy density by

$$\psi(\mathbf{E}, D) = \phi(D) W_0(\mathbf{E}) \quad (6)$$

Grinfeld assumed ϕ to be linearly related to D according to

$$\phi(D) = 1 - (1 - \phi_{\min})D \quad (7)$$

where ϕ_{\min} is a second material constant introduced by the model (C in equation 5 was the first). Equation 7 is sketched in Figure 2. This dimensionless constant ϕ_{\min} is used to specify the residual stiffness of fully damaged material. ϕ_{\min} satisfies the restriction

$$0 \leq \phi_{\min} \leq 1 \quad (8)$$

The lower limit corresponds to the case of zero residual stiffness and the upper limit to the case of no degradation of stiffness. Combination of equations 5, 6, and 7 yields

$$\dot{D} = (1 - \phi_{\min})C \cdot \mu \left(\frac{\nu}{1 - 2\nu} E_{ii} E_{jj} + E_{ij} E_{ij} \right) \quad (9)$$

Calculation of Stresses

Coleman and Gurtin [6] established a relationship between stress and the Helmholtz free energy that follows as a consequence of applying the Clausius-Duhem Inequality to a material model involving internal state variables. In our special case of a single internal state variable D and small deformations, Coleman and Gurtin showed equation 3 to be generalizable to

$$S_{ij} = \frac{\partial \psi}{\partial E_{ij}} \quad (10)$$

From equation 6,

$$S_{ij} = \phi(D) \frac{\partial W_0}{\partial E_{ij}} \quad (11)$$

Combination of equations 1 and 11 yields the stress-strain relation

$$S_{ij} = 2 \cdot \phi(D) \cdot \mu \left(\frac{\nu}{1 - 2\nu} E_{kk} \delta_{ij} + E_{ij} \right) \quad (12)$$

The components of the second Piola Kirchhoff stress tensor are then

$$S_{xx} = \phi(D) \frac{2\mu}{1-2\nu} [(1-\nu)E_{xx} + \nu(E_{yy} + E_{zz})] \quad (13a)$$

$$S_{yy} = \phi(D) \frac{2\mu}{1-2\nu} [(1-\nu)E_{yy} + \nu(E_{xx} + E_{zz})] \quad (13b)$$

$$S_{zz} = \phi(D) \frac{2\mu}{1-2\nu} [(1-\nu)E_{zz} + \nu(E_{xx} + E_{yy})] \quad (13c)$$

$$S_{xy} = \phi(D) 2\mu E_{xy} \quad (13d)$$

$$S_{yz} = \phi(D) 2\mu E_{yz} \quad (13e)$$

$$S_{zx} = \phi(D) 2\mu E_{zx} \quad (13f)$$

In summation, the Grinfeld damage model can be described as follows. The undamaged material is governed by isotropic linear elasticity, equation 4. Damage variable D evolves according to equation 9. As it does, the degradation function ϕ decreases according to equation 7. Stress components are then determined from equations 13. In effect, the elastic shear modulus, μ , is degraded and Poisson's ratio is unchanged.

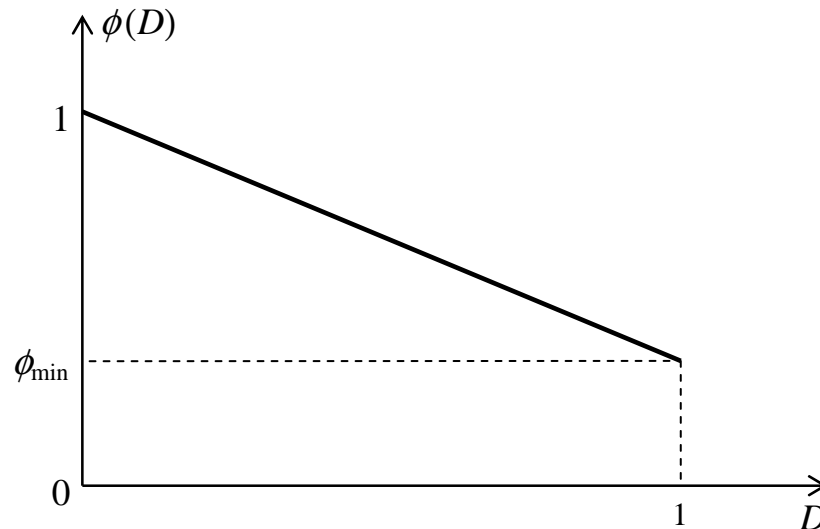


Figure 2. Degradation Function $\phi(D)$.

Damage Model Implementation into LS-DYNA

Use of *MAT_USER_DEFINED_MATERIAL_MODELS

The Grinfeld damage model was installed in LS-DYNA version 971 by means of the feature *MAT_USER_DEFINED_MATERIAL_MODELS. The implementation uses one “history variable” for damage D , and the material array “CM” contains the material constants ρ , μ , ν , C , and ϕ_{\min} . A subroutine was written that is called every time step individually for each element. The parameter IHYPER is set to 1, so that the code passes the deformation gradient tensor, \mathbf{F} , to the user’s subroutine. The flow of calculations in the subroutine is as follows.

The subroutine computes Green strain using

$$\mathbf{E} = \frac{1}{2}(\mathbf{F}^T \cdot \mathbf{F} - \mathbf{I}) \quad (14)$$

instead of in an incremental, *hypoelastic* way using the element’s strain increments for that time step that are passed to the subroutine via the arguments on the first line. Damage D is then computed using a first-order integration of equation 9,

$$D(t) = D(t - \Delta t) + (1 - \phi_{\min}) C \mu \left(\frac{\nu}{1 - 2\nu} E_{ii} E_{jj} + E_{ij} E_{ij} \right) \Delta t \quad (15)$$

where Δt is the time step. Equation 7 is used to compute ϕ . Equations 13 are used to evaluate components of the second Piola-Kirchhoff stress, \mathbf{S} . Finally, Cauchy stress, $\boldsymbol{\sigma}$, is computed using

$$\boldsymbol{\sigma} = \frac{\mathbf{F} \cdot \mathbf{S} \cdot \mathbf{F}^T}{\det \mathbf{F}} \quad (16)$$

The element’s six components of Cauchy stress are returned to the code via the argument list.

Testing the Implementation

The implementation was tested by means of three single-element problems: uniaxial tension at a constant stretch rate, uniaxial tension at a constant stretch rate with superimposed rigid-body rotation, uniaxial compression at a constant stretch rate, and uniaxial tension at a constant stretch rate with superimposed rigid-body rotation.

Figure 3 shows a single 8-node brick element. Note the material and spatial coordinate systems defined in the figure. The shape function of this 8-node element restricts its internal velocity field to the following quadratic form in x , y , and z .

$$v_x(x, y, z, t) = a_x(t) + b_x(t)x + c_x(t)y + d_x(t)z + e_x(t)xy + f_x(t)xz + g_x(t)yz \quad (17a)$$

$$v_y(x, y, z, t) = a_y(t) + b_y(t)x + c_y(t)y + d_y(t)z + e_y(t)xy + f_y(t)xz + g_y(t)yz \quad (17b)$$

$$v_z(x, y, z, t) = a_z(t) + b_z(t)x + c_z(t)y + d_z(t)z + e_z(t)xy + f_z(t)xz + g_z(t)yz \quad (17c)$$

v_x , v_y , and v_z are the three components of velocity. The coefficients $a_x(t), b_x(t), \dots, g_z(t)$ are functions only of time.

At time $t = 0$, the element in Figure 3 is a cube with edge length L_0 . Thereafter, a time-independent x -velocity v_0 is imposed on the four nodes of the face $X = L_0$. At these same four nodes, the y - and z -velocities are held at zero. At the four nodes of the opposite face, defined by $X = 0$, all three velocity components are held at zero. The boundary conditions of the problem are therefore

$$v_x(L_0, Y, Z, t) = v_0 t \quad (18a)$$

$$v_x(0, Y, Z, t) = v_y(0, Y, Z, t) = v_z(0, Y, Z, t) = v_y(L_0, Y, Z, t) = v_z(L_0, Y, Z, t) = 0 \quad (18b)$$

Once conditions 18a and 18b are imposed on the shape functions of equations 17a–c, we find that motion throughout the element is described by the mapping

$$x(X, t) = X + \frac{v_0 t}{L_0} X = \left(1 + \frac{v_0 t}{L_0}\right) X \quad (19a)$$

$$y = Y \quad (19b)$$

$$z = Z \quad (19c)$$

Equations 19a–c are exact regardless of how fast one pulls the element. There are no inertia effects in this single-element problem, which makes it a useful vehicle for isolating effects of the constitutive model.

Thus the deformation gradient tensor is

$$\mathbf{F}(\mathbf{t}) = \frac{\partial \mathbf{x}}{\partial \mathbf{X}} = \begin{bmatrix} 1 + \frac{v_0 t}{L_0} & 0 & 0 \\ 0 & 1 & 0 \\ 0 & 0 & 1 \end{bmatrix} \quad (20)$$

and the Green strain tensor is

$$\mathbf{E}(\mathbf{t}) = \frac{1}{2}(\mathbf{F}^T \cdot \mathbf{F} - \mathbf{I}) = \begin{bmatrix} \frac{v_0 t}{L_0} \left(1 + \frac{v_0 t}{2L_0}\right) & 0 & 0 \\ 0 & 0 & 0 \\ 0 & 0 & 0 \end{bmatrix} \quad (21)$$

Note that the strain is spatially constant throughout the element. If the strain is small, then there is little difference between strain and stretch, i.e.,

$$E_{xx}(t) = \frac{v_0 t}{L_0} \left(1 + \frac{v_0 t}{2L_0} \right) \cong \frac{v_0 t}{L_0} \quad (22)$$

and our constant stretch rate corresponds approximately to a constant strain rate; call it \dot{E} .

$$\dot{E}_{xx} \cong \frac{v_0}{L_0} \equiv \dot{E} \quad (23)$$

The elastic strain energy density throughout the element is then

$$W_0(t) = \mu \left(\frac{\nu}{1-2\nu} E_{ii} E_{jj} + E_{ij} E_{ij} \right) \cong \frac{(1-\nu)\mu}{1-2\nu} (E_{xx}(t))^2 = \frac{(1-\nu)\mu}{1-2\nu} (\dot{E}t)^2 \quad (24)$$

The damage evolution equation becomes

$$\frac{dD}{dt} = (1 - \phi_{\min}) C \cdot W_0(t) = (1 - \phi_{\min}) C \cdot \frac{(1-\nu)\mu}{1-2\nu} (\dot{E}t)^2 \quad (25)$$

The solution, assuming no initial damage at time zero, is the cubic in time

$$D(t) = (1 - \phi_{\min}) C \cdot \frac{(1-\nu)\mu}{3(1-2\nu)} \cdot \dot{E}^2 t^3 \quad (26)$$

However, this solution must be modified to take account of the upper bound of 1, reached at some time t^* determined from

$$D(t^*) = (1 - \phi_{\min}) C \cdot \frac{(1-\nu)\mu}{3(1-2\nu)} \cdot \dot{E}^2 (t^*)^3 = 1$$

to be

$$t^* = \left[\frac{1}{(1 - \phi_{\min}) C} \cdot \frac{3(1-2\nu)}{(1-\nu)\mu} \right]^{1/3} \cdot \dot{E}^{-2/3} \quad (27)$$

This provides a time scale associated with damage evolution. The time scale decreases with increasing strain rate. The two-part solution for D is then

$$D(t) = \begin{cases} \left(\frac{t}{t^*}\right)^3 & ; \quad 0 \leq t < t^* \\ 1 & ; \quad t \geq t^* \end{cases} \quad (28)$$

The degradation function is

$$\phi(t) = 1 - (1 - \phi_{\min})D = \begin{cases} 1 - (1 - \phi_{\min})\left(\frac{t}{t^*}\right)^3 & ; \quad 0 \leq t < t^* \\ \phi_{\min} & ; \quad t \geq t^* \end{cases} \quad (29)$$

In order to calculate stress, we return to Equation 24.

$$W_0 = \frac{(1-\nu)\mu}{1-2\nu} \cdot E_{xx}^2 \quad (30)$$

Then

$$S_{xx} = \phi(D) \frac{\partial W_0}{\partial E_{xx}} = \phi(D) \cdot \frac{2(1-\nu)\mu}{1-2\nu} \cdot E_{xx}$$

From equation 22,

$$S_{xx}(t) = \phi(t) \cdot \frac{2(1-\nu)\mu}{1-2\nu} \cdot \dot{E}t$$

so that

$$S_{xx}(t) = \frac{2(1-\nu)\mu}{1-2\nu} \cdot \dot{E}t \cdot \begin{cases} \left[1 - (1 - \phi_{\min})\left(\frac{t}{t^*}\right)^3 \right] & ; \quad 0 \leq t < t^* \\ \phi_{\min} & ; \quad t \geq t^* \end{cases} \quad (31)$$

In Figure 4, equations 22, 28, and 31 have been evaluated using the material properties in Table 1. In addition the same problem was modeled using LS-DYNA and the numerical results were virtually indistinguishable from the analytical results plotted in Figure 4.

Table 1. Parameter values used in Figure 4.

ρ (kg/m ³)	3215.
μ (GPa)	193.0
ν	0.1606
C (m·s/kg)	1.0×10^{-5}
ϕ_{\min}	0.1
L_0 (m)	0.01
v_0 (m/s)	8.0×10^{-4}

In Figure 5, equation 31 for S_{XX} is evaluated for the case of no damage ($C = 0$), and the result is compared with the previous evaluation for $C = 1.0 \times 10^{-5}$ m·s/kg. We see that the damage model has substantially reduced the stress levels attained.

Next the direction of v_0 in Figure 3 is reversed, so that a constant stretch-rate uniaxial compression test is performed. Figure 6 shows the results for D and S_{XX} vs. t .

The D results in Figure 6 are identical to those in Figure 4 from the tension test. Equation 35 is quadratic in strain rate and so does not distinguish tension from compression. Ultimately this feature stems from the hypothesis of the damage model that the rate of damage growth is proportional to the strain energy, which is quadratic in the strain components.

Nevertheless, the stresses that develop in the compression test are properly compressive. Note that, for a given absolute value of E_{XX} , the value of S_{XX} in Figure 6 is equal in magnitude and opposite in sign to its counterpart in Figure 4.

Finally, the element in Figure 3 is stretched along its X axis at a constant stretch rate, but now we superimpose rigid-body about the z axis at a constant angular velocity. Material constant $C = 0$, so that damage is turned off and the model reduces to linear elasticity. Figure 7b compares the second Piola-Kirchhoff stress, S_{XX} , and the Cauchy stress, σ_{xx} , as functions of time. Note that S_{XX} increases proportionally with E_{XX} , but σ_{xx} is affected by the rigid-body rotation. The property of *frame indifference*, also called *material objectivity*, is most easily imposed on a material model by stating that model as a relationship between Green strain and second Piola-Kirchhoff stress.

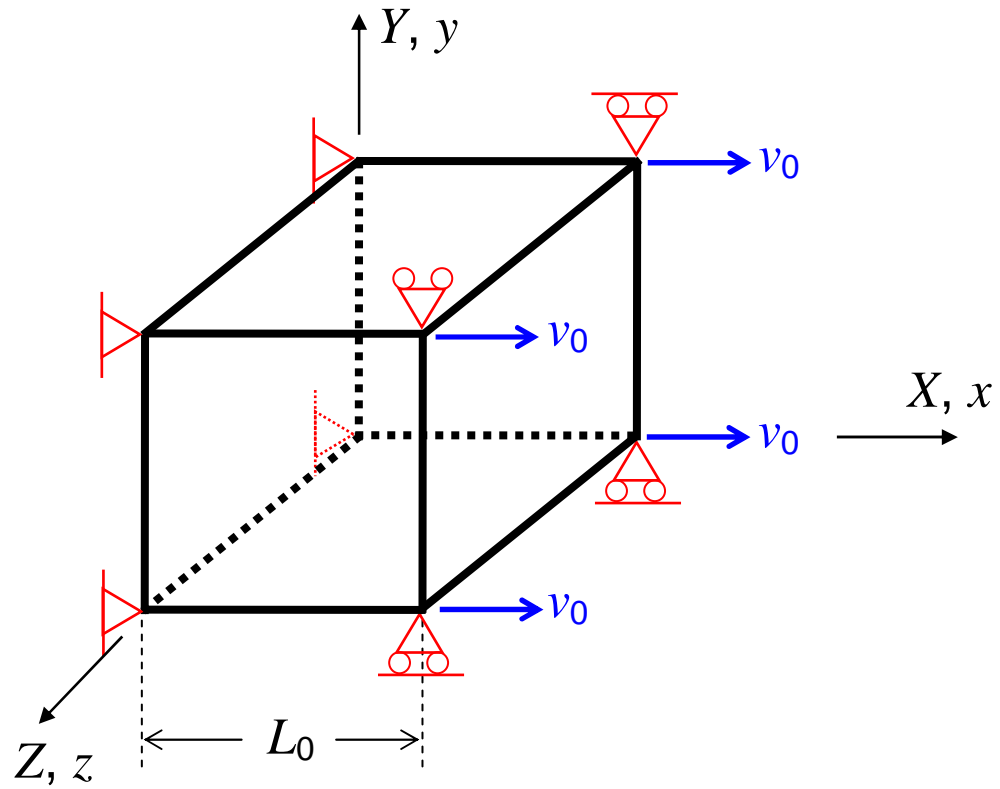
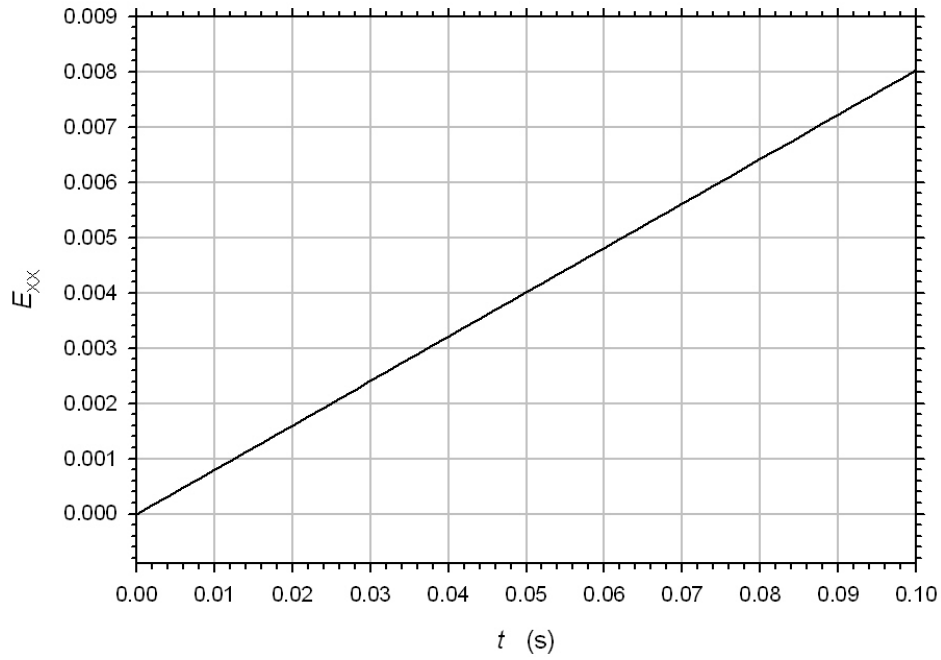


Figure 3. An 8-node brick finite element subjected to uniaxial strain.

(a)



(b)

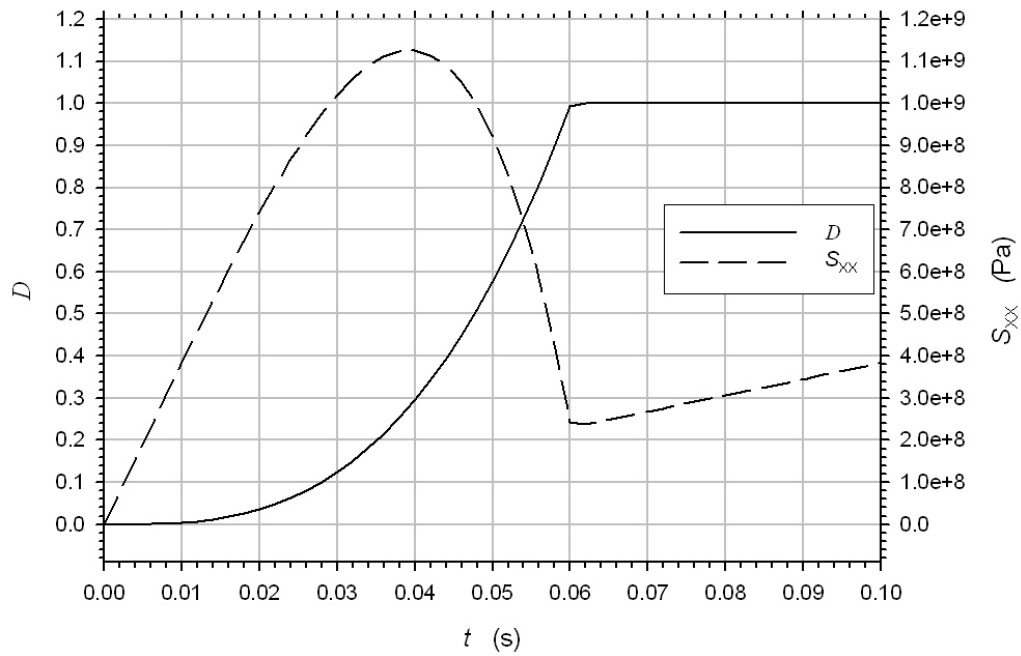


Figure 4. (a) The element in Figure 3 is stretched at a constant positive (tensile) rate, and (b) D and S_{XX} evolve.

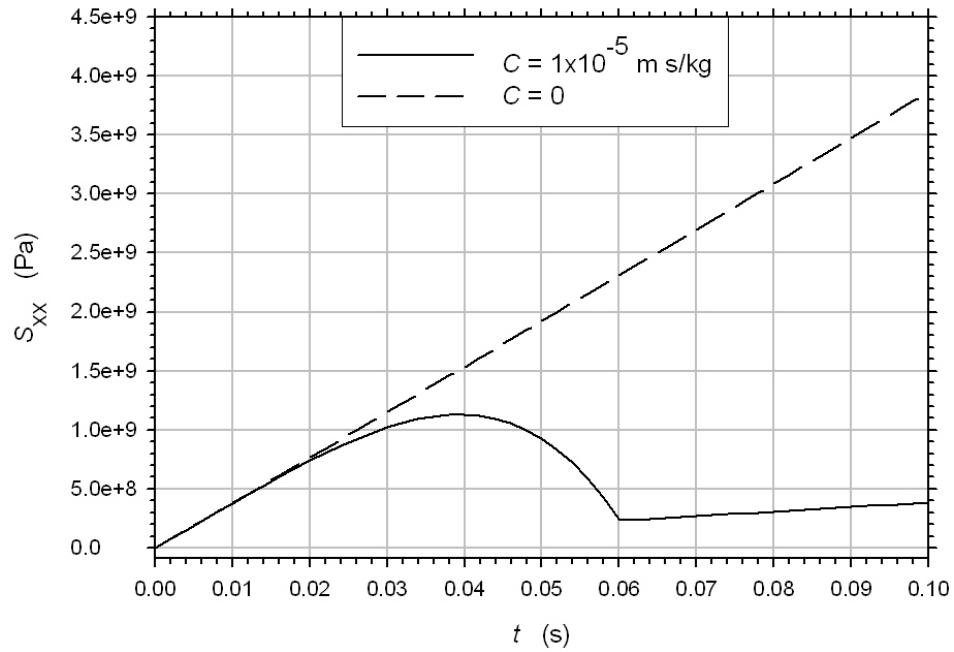
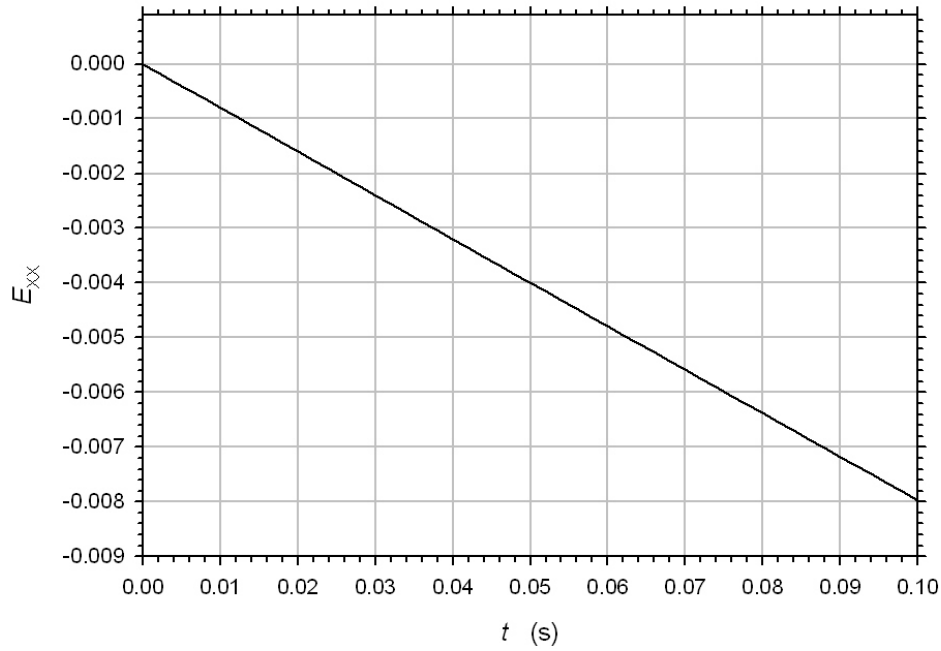


Figure 5. The solution to the problem in Figure 3 evaluated with and without damage.

(a)



(b)

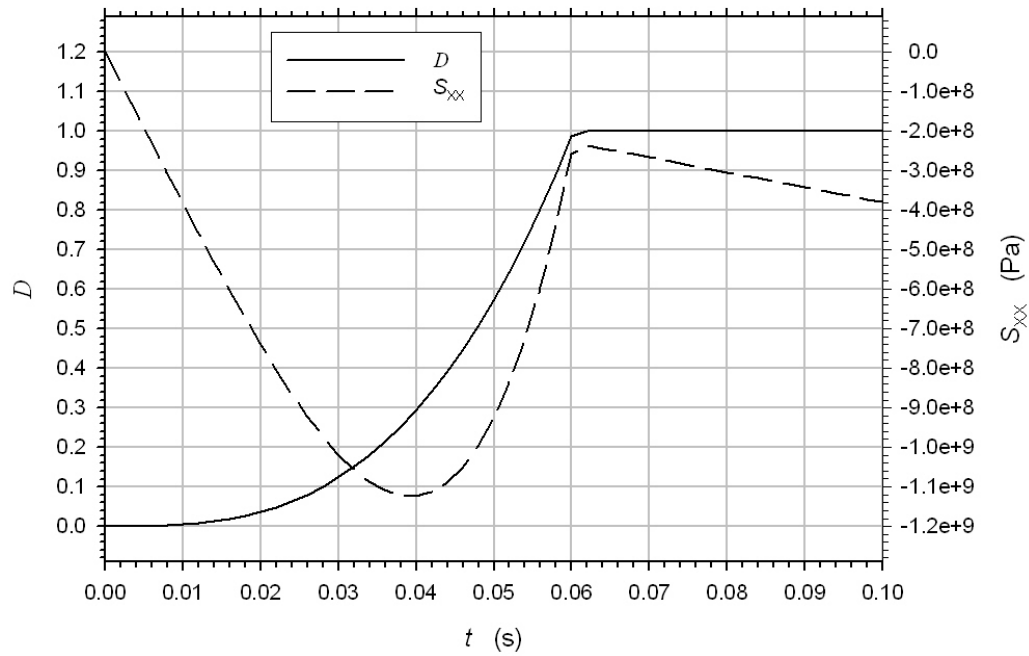
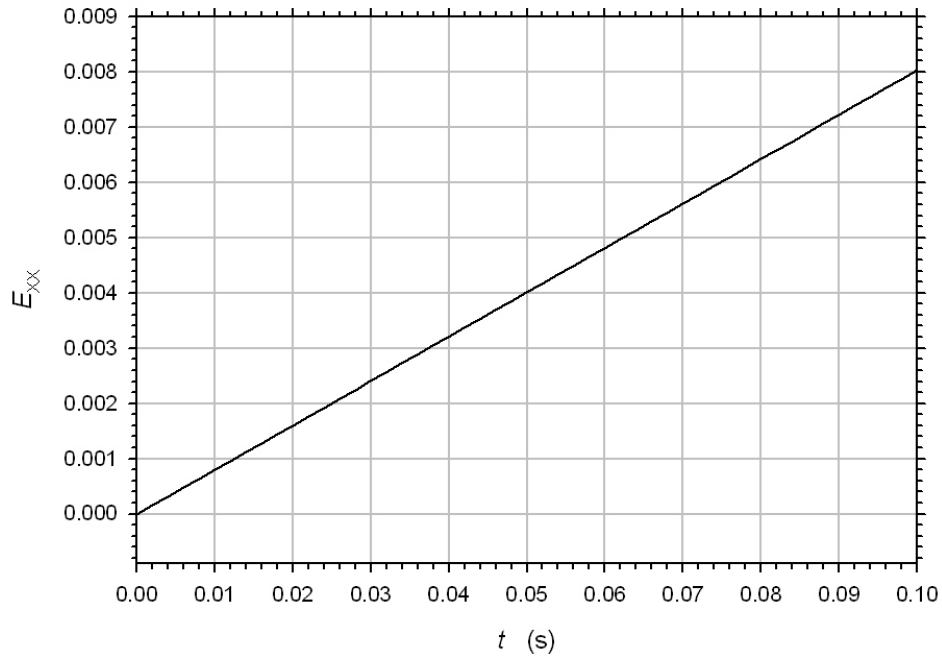


Figure 6. (a) The element in Figure 3 is compressed at a constant negative stretch rate, and (b) D and S_{xx} evolve.

(a)



(b)

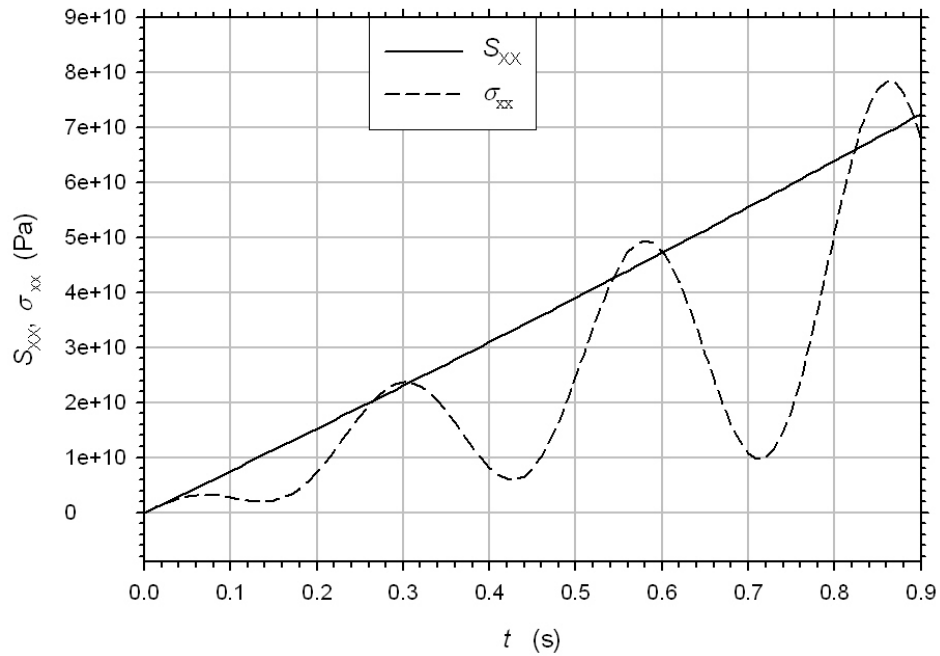


Figure 7. (a) The element in Figure 3 is stretched along the x direction at a constant positive rate, this time with a superimposed rigid-body rotation at a constant angular velocity about the z axis. Material constant $C = 0$, so that damage is turned off. (b) S_{xx} and σ_{xx} differ substantially.

Application to Normal Plate-on-Plate Impact

The Initial-Value, Boundary-Value Problem

In normal plate-on-plate impact, a flyer plate is launched at a certain velocity into a stationary target plate. For the purpose of analytical work “on paper,” we apply small strain and small displacement theory, a reasonable approximation in tests performed on glass. Hence, we neglect any distinctions between material coordinate \mathbf{X} and spatial coordinate \mathbf{x} , between Green strain \mathbf{E} and infinitesimal strain \mathbf{e} , and between second Piola-Kirchhoff stress \mathbf{S} and Cauchy stress $\boldsymbol{\sigma}$.

At time $t = 0$, $x = 0$ defines the impacted face of the target plate and $x = L$, where L is the initial thickness of the target plate, defines the free surface. Let u_x , u_y , and u_z be the three components of displacement. Throughout the central portion of the target plate, i.e., the region of sufficiently small y and z ,

$$u_y \equiv u_z \equiv 0 \quad (32a)$$

$$\frac{\partial u_x}{\partial y} \equiv \frac{\partial u_x}{\partial z} \equiv 0 \quad (32b)$$

In the central region, the only component of strain not identically zero is related to the displacement field by

$$e_{xx} = \frac{\partial u_x}{\partial x} \quad (33)$$

Equations 13 determine the components of stress.

$$\sigma_{xx} = \phi(D) \cdot \frac{2(1-\nu)\mu}{1-2\nu} e_{xx} \quad (34a)$$

$$\sigma_{yy} = \sigma_{zz} = \phi(D) \cdot \frac{2\nu\mu}{1-2\nu} e_{xx} \quad (34b)$$

$$\sigma_{xy} \equiv \sigma_{yz} \equiv \sigma_{zx} \equiv 0 \quad (34c)$$

Equation 9 for damage evolution reduces to

$$\frac{\partial D}{\partial t} = (1 - \phi_{\min}) C \cdot \frac{(1-\nu)\mu}{1-2\nu} \cdot e_{xx}^2 \quad (35)$$

To this we add the x -momentum equation

$$\rho \frac{\partial^2 u_x}{\partial t^2} = \frac{\partial \sigma_{xx}}{\partial x} \quad (36)$$

The boundary conditions are sketched in Figure 8a. On the impacted face at $x = 0$, a time-independent velocity v_0 is prescribed. On the free surface at $x = L$, zero normal stress is prescribed. Homogeneous initial conditions are imposed on displacement, velocity, and damage D .

Equations 33, 34a, 35, and 36 are combined to yield two coupled nonlinear partial differential equations in two unknowns, u_x and D . These equations and the boundary and initial conditions constitute the following initial value, boundary value problem (IVBVP).

DE

$$\frac{1}{c_0^2} \frac{\partial^2 u_x}{\partial t^2} = \frac{\partial^2 u_x}{\partial x^2} - (1 - \phi_{\min}) \left(D \frac{\partial^2 u_x}{\partial x^2} + \frac{\partial D}{\partial x} \frac{\partial u_x}{\partial x} \right) \quad (37)$$

$$\frac{\partial D}{\partial t} = (1 - \phi_{\min}) C \cdot \frac{(1 - \nu)\mu}{1 - 2\nu} \left(\frac{\partial u_x}{\partial x} \right)^2 \quad (38)$$

BC

$$\frac{\partial u_x}{\partial t}(0, t) = v_0, \quad \frac{\partial u_x}{\partial x}(L, t) = 0 \quad (39)$$

IC

$$u_x(x, 0) = 0, \quad \frac{\partial u_x}{\partial t}(x, 0) = 0, \quad D(x, 0) = 0 \quad (40)$$

The domain is

$$x \in [0, L], \quad t \geq 0 \quad (41)$$

The parameter c_0 appearing in equation 37 is defined by

$$c_0 = \sqrt{\frac{2(1 - \nu)\mu}{(1 - 2\nu)\rho}} \quad (42)$$

Scaling the IVBVP

The dimensionless quantities \hat{x} , \hat{t} , \hat{u}_x , \hat{v}_x , and $\hat{\sigma}_{xx}$ are defined by

$$\hat{x} = \frac{x}{L}, \quad \hat{t} = \frac{c_0 t}{L}, \quad \hat{u}_x = \frac{c_0 u_x}{v_0 L}, \quad \hat{v}_x = \frac{v_x}{v_0}, \quad \hat{\sigma}_{xx} = \frac{\sigma_{xx}}{\rho c_0 v_0} \quad (43)$$

These are substituted into equations 37–41 to yield the scaled IVBVP

DE

$$\frac{\partial^2 \hat{u}_x}{\partial \hat{t}^2} = \frac{\partial^2 \hat{u}_x}{\partial \hat{x}^2} - (1 - \phi_{\min}) \left(D \frac{\partial^2 \hat{u}_x}{\partial \hat{x}^2} + \frac{\partial D}{\partial \hat{x}} \frac{\partial \hat{u}_x}{\partial \hat{x}} \right) \quad (44)$$

$$\frac{\partial D}{\partial \hat{t}} = \Pi \cdot \left(\frac{\partial \hat{u}_x}{\partial \hat{x}} \right)^2 \quad (45)$$

BC

$$\frac{\partial \hat{u}_x}{\partial \hat{t}}(0, \hat{t}) = 1, \quad \frac{\partial \hat{u}_x}{\partial \hat{x}}(1, \hat{t}) = 0 \quad (46)$$

IC

$$\hat{u}_x(\hat{x}, 0) = 0, \quad \frac{\partial \hat{u}_x}{\partial \hat{t}}(\hat{x}, 0) = 0, \quad D(\hat{x}, 0) = 0 \quad (47)$$

$$\hat{x} \in [0, 1], \quad \hat{t} \geq 0 \quad (48)$$

in which

$$\Pi = (1 - \phi_{\min}) C \cdot \frac{\rho}{2c_0} \cdot L \cdot v_0^2 \quad (49)$$

This scaled IVBVP involves only two dimensionless parameters, ϕ_{\min} and Π . This greatly reduces the computational “test matrix.”

Dimensionless Parameter Π

Π is proportional to C and is a dimensionless measure of the material’s damage sensitivity. For soda lime glass, Ref. [2] gives $\rho = 2500 \text{ kg/m}^3$ and $c_0 = 5840 \text{ m/s}$. Choose $\phi_{\min} = 0.1$. The target plate thickness is typically a few millimeters, so $L \approx 0.005 \text{ m}$. One-half the flyer plate speed, applicable for symmetric impact, is typically a few hundred meters per second, so $v_0 \approx 300 \text{ m/s}$. Thus,

$$\Pi \approx 86.7 \frac{\text{kg}}{\text{m} \cdot \text{s}} \cdot C \quad (50)$$

LS-DYNA Results for Various Π

The IVBVP in equations 44–48 can be solved for arbitrary Π by means of the LS-DYNA implementation. In the finite element mesh employed, the length between $\hat{x} = 0$ and $\hat{x} = 1$ was divided into 16000 8-node brick elements. The uniaxial displacement condition was imposed by means of constraints on the boundary nodes. Gaussian quadrature was performed with one integration point per element. Default artificial viscosity coefficients were used: quadratic viscosity Q1 = 1.5, linear viscosity Q2 = 0.06, hourglass coefficient QH = 0.1.

The solution was initially obtained for $\Pi = 0, 0.1, 0.2, 0.3,$ and 0.4 and for $\phi_{\min} = 0.1$. Figure 9 shows the computed spatial distributions of D and ϕ through the target plate's thickness. These profiles are plotted at time $\hat{t} = 1.5$, chosen to estimate the time at which the unloading wave should encounter the damage front according to the hypothesis sketched in Figure 1b. Note that changes in ϕ are broadly distributed across the thickness and do not occur abruptly at a specific location.

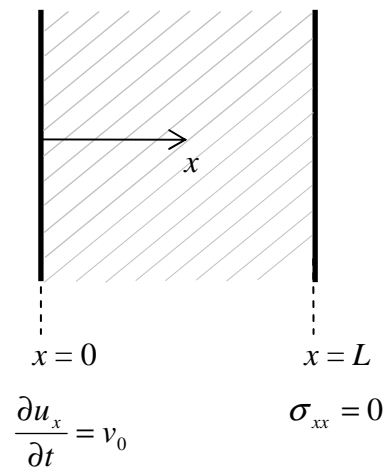
Figure 10 shows the results for $\hat{v}_x(1, \hat{t})$, the free-surface normal velocity as a function of time. The compressive shock arrives at $\hat{t} = 1$. For $\Pi = 0$, the scaled velocity jumps to 2 and remains at that level until $\hat{t} = 3$. As Π is increased successively to 0.1, 0.2, 0.3, and 0.4, the free-surface velocity jumps at $\hat{t} = 1$ to ever decreasing levels. Furthermore, for $\Pi > 0$ the free-surface velocity does not remain constant throughout the duration $\hat{t} \in (1, 3)$. The slight increase in velocity with time for $\Pi = 0.1$ and 0.2 indicates the arrival of a partially reflected unloading wave. However, this velocity rise is gradual over time and the computed free-surface velocity does not exhibit the distinct second plateau of Figure 1a.

Figure 11 compares $\hat{v}_x(1, \hat{t} = 1.125)$ and $\hat{v}_x(1, \hat{t} = 2.000)$ as a function of Π ; their difference provides a convenient indicator of whether the free-surface velocity increases or decreases following the arrival of the initial shock wave. We see that $[\hat{v}_x(\hat{x} = 1, \hat{t} = 2.000) - \hat{v}_x(\hat{x} = 1, \hat{t} = 1.125)]$ peaks at $\Pi = 0.126$. In Figure 12 we see the free-surface velocity gradually rising over time for $\Pi = 0.126$.

The solution for stress corresponding to $\Pi = 0.126$ is examined in Figure 13. We see that one effect of damage has been to *decrease the stress-wave speed*. The compressive loading wave front during $\hat{t} \in (0, 1)$ traverses the undamaged target plate with a scaled speed very nearly equal to 1, but during $\hat{t} \in (1, 2)$ the unloading wave front travels back into the damaged material with a speed smaller than 1. A second effect of damage has been to *decrease the amplitude of the stress signal*. In Figure 13 the lightening blue color at $\hat{t} = 1.75$ and $\hat{t} = 2.00$ near the impact face at $\hat{x} = 0$ indicates a reduced stress amplitude.

Figure 14 shows damage contours in $\hat{x} - \hat{t}$ space. This figure also displays the location of the stress-wave front, which is identified with the location of the maximum value of $|d\hat{\sigma}_{xx}/d\hat{x}|$. Figure 14 depicts the reduction in the stress front's speed for $\hat{t} > 1$ by displaying the $(L - c_0 t)$ line.

(a)



(b)

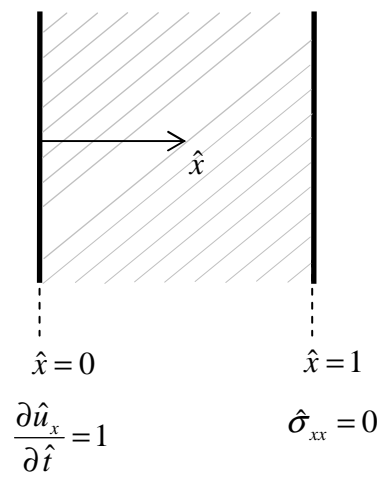


Figure 8. The boundary conditions imposed on the target in the uniaxial strain model of normal plate-on-plate impact (a) before and (b) after scaling.

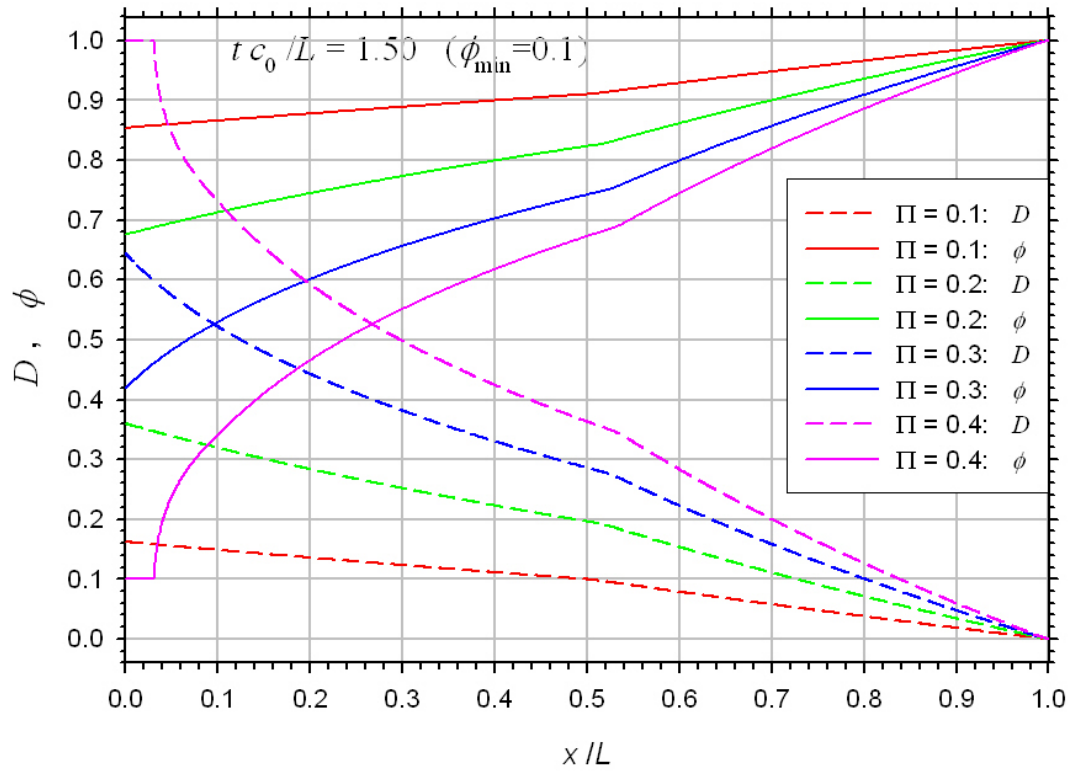


Figure 9. D and ϕ as functions of \hat{x} at $\hat{t} = 1.5$ and for various Π . ($\phi_{\min} = 0.1$.)

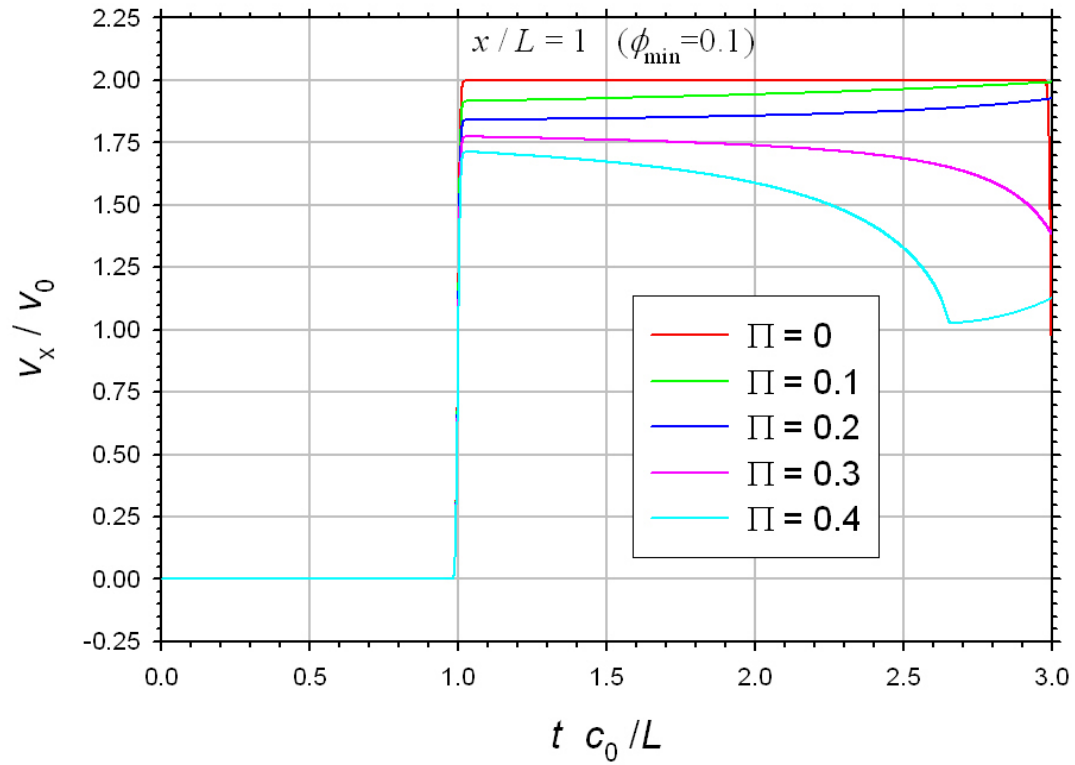


Figure 10. \hat{v}_x at $\hat{x} = 1$ (the free-surface normal velocity) as a function of \hat{t} and for various Π .
($\phi_{\min} = 0.1$.)

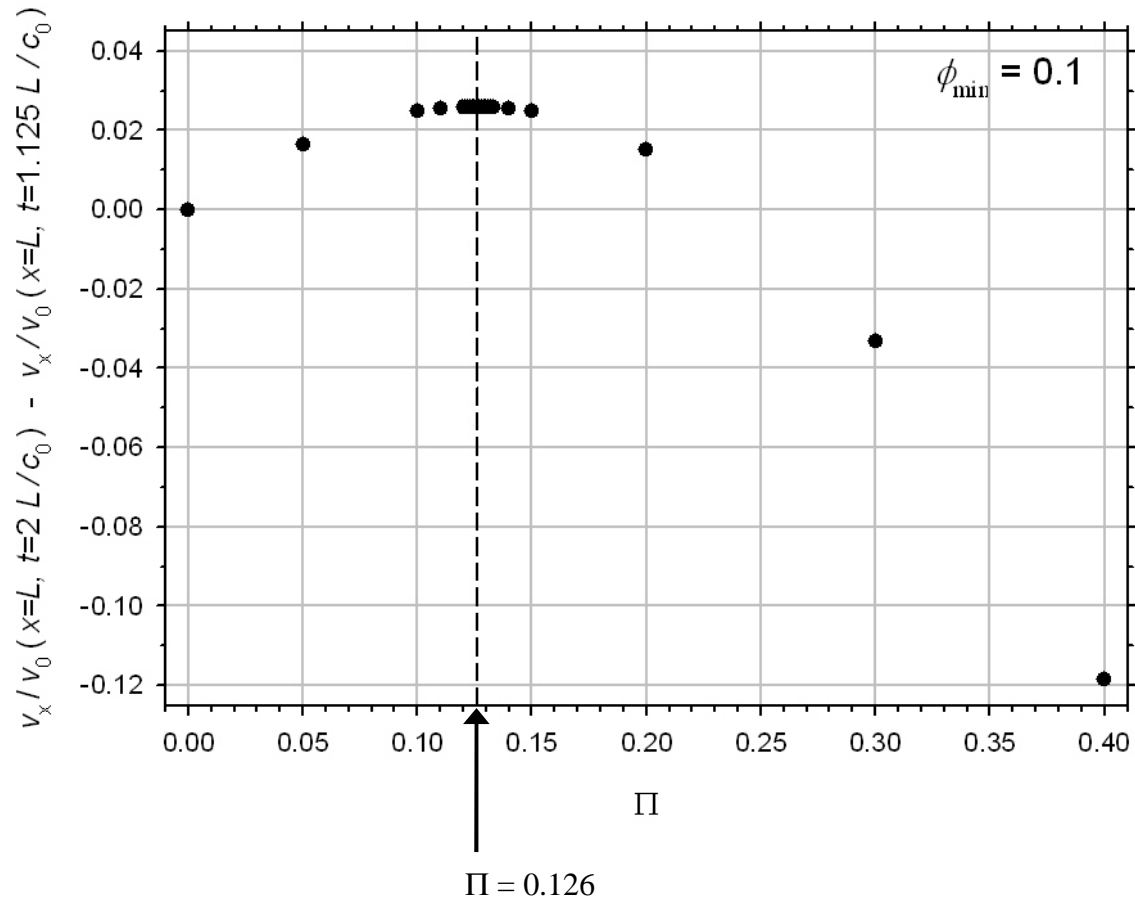


Figure 11. $\hat{v}_x(\hat{x}=1, \hat{t}=2.000) - \hat{v}_x(\hat{x}=1, \hat{t}=1.125)$ as a function of Π . ($\phi_{\min} = 0.1$.) The maximum value at $\Pi = 0.126$ is noted.

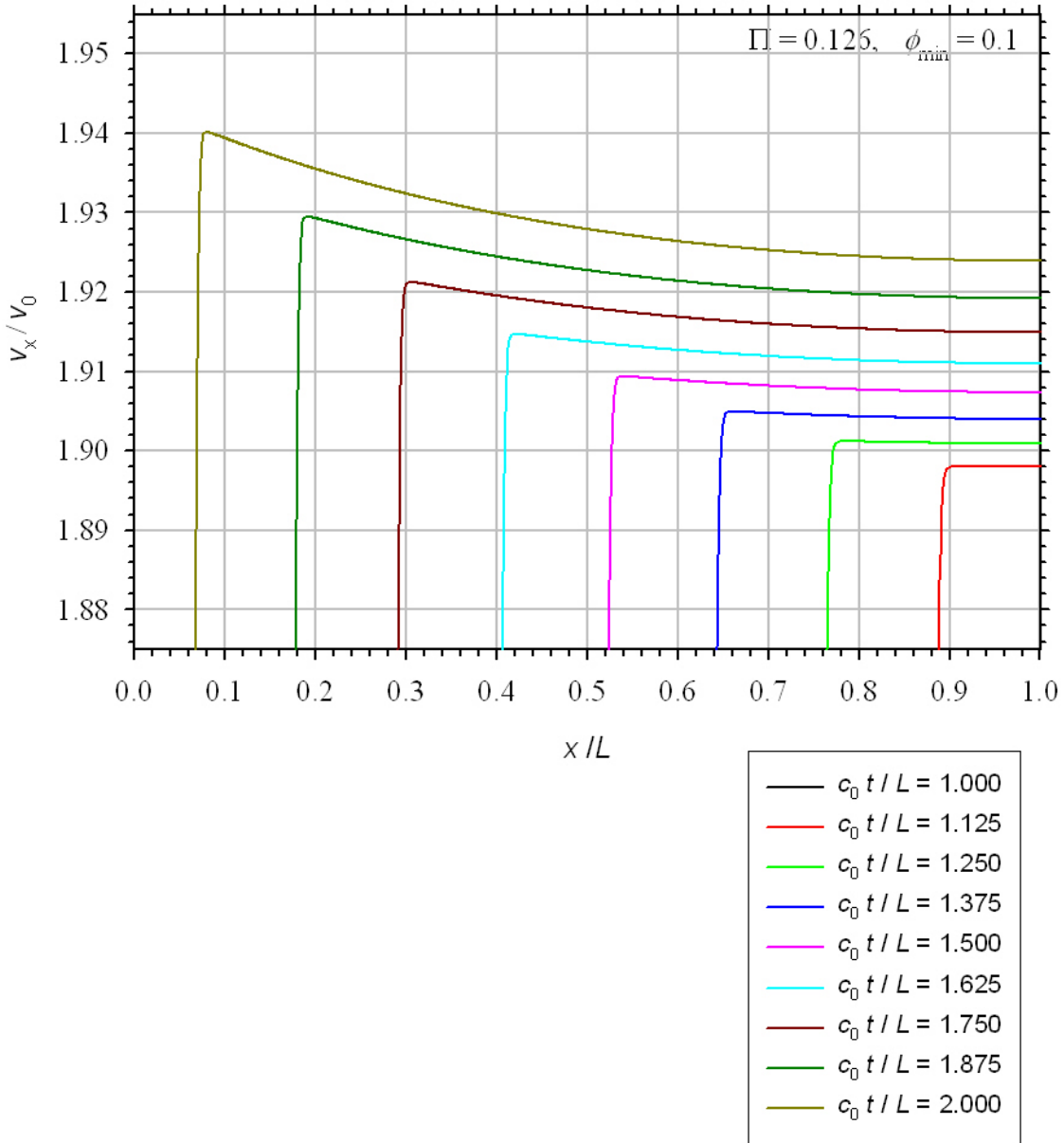


Figure 12. \hat{v}_x as a function of \hat{x} for various $\hat{t} \in [1,2]$ and for $\Pi = 0.126$. ($\phi_{\min} = 0.1$.)

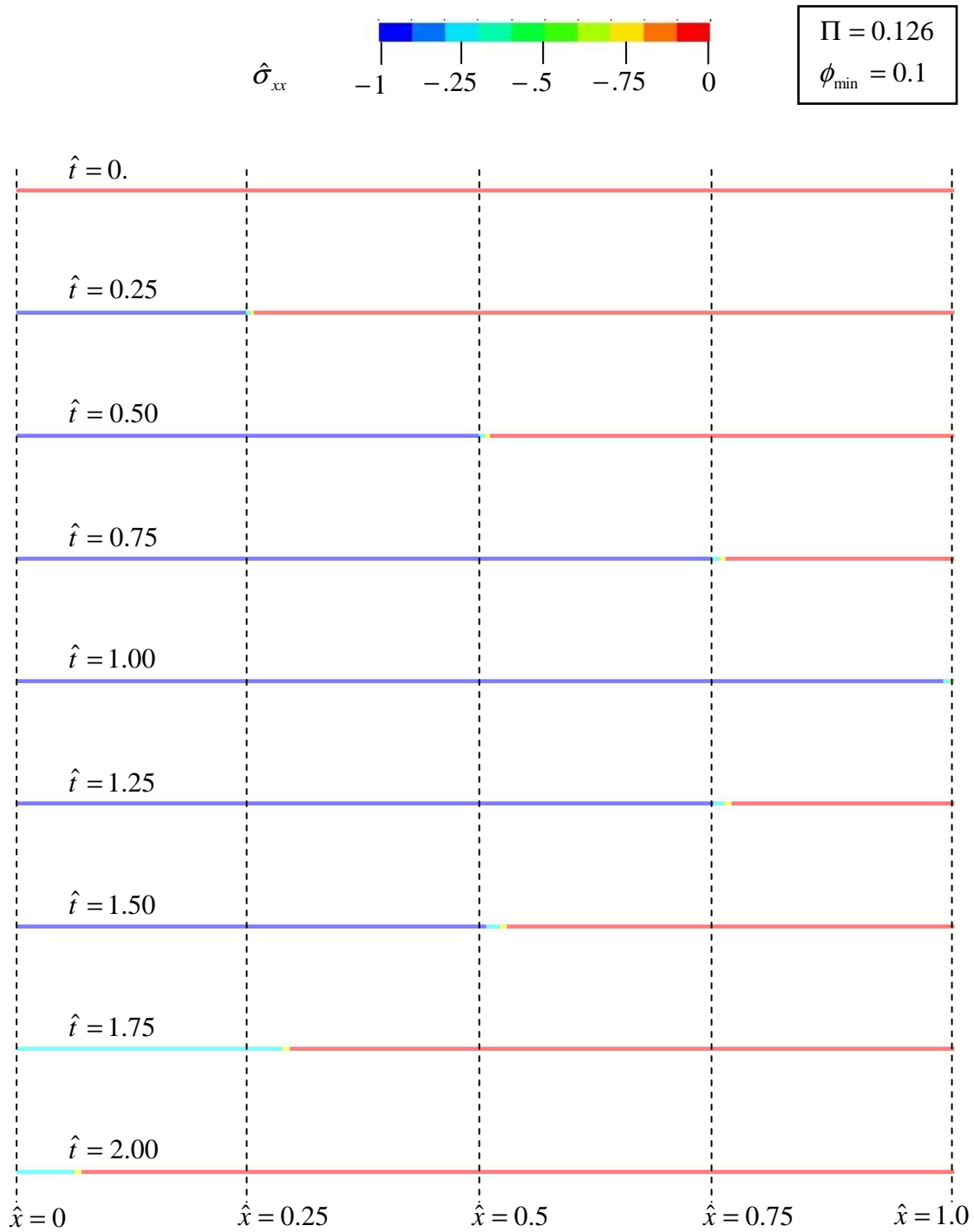


Figure 13. Contours of $\hat{\sigma}_{xx}$ across the target plate for $\Pi = 0.126$. ($\phi_{\min} = 0.1$.)

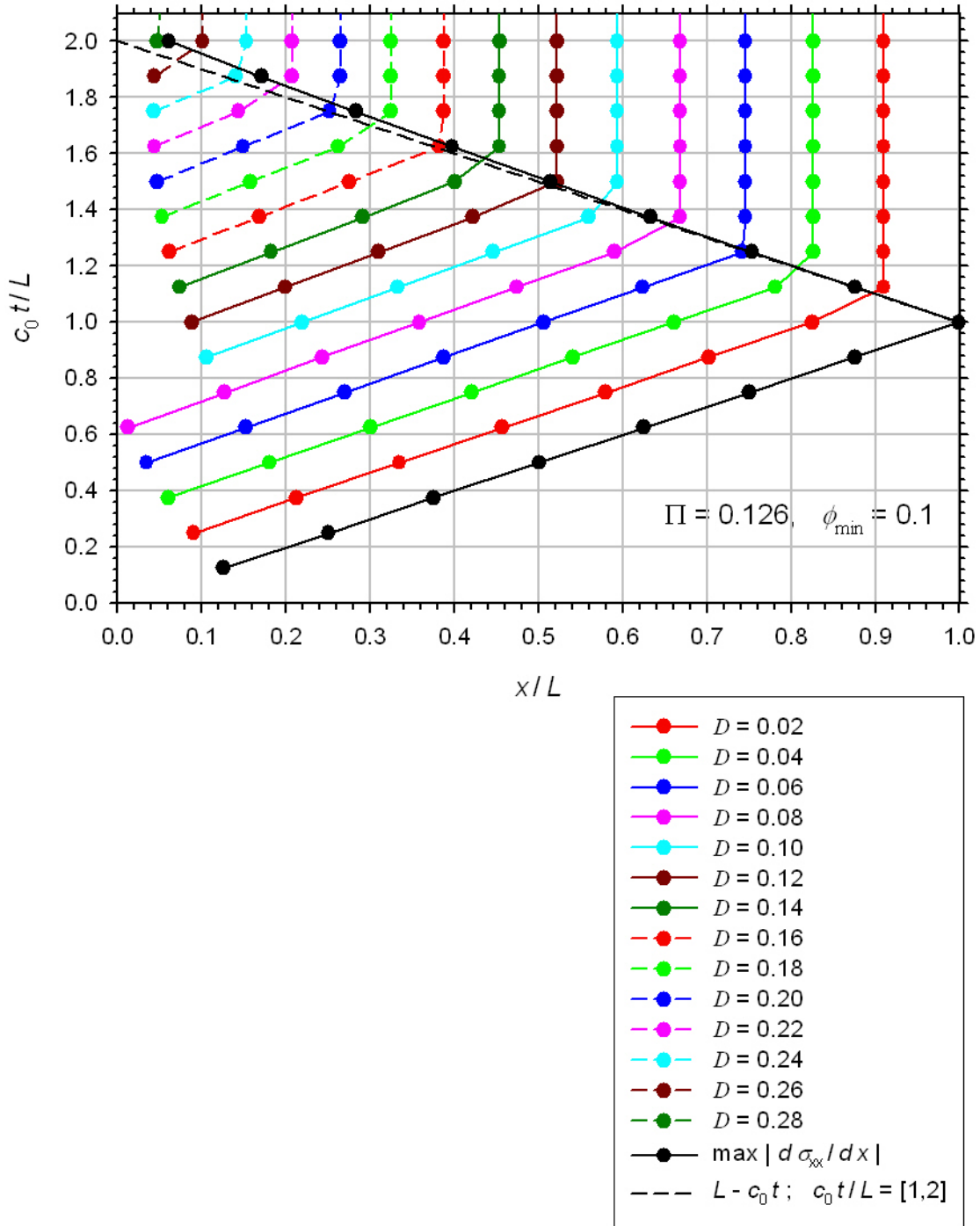


Figure 14. D Contours in \hat{x} - \hat{t} space for $\Pi = 0.126$. ($\phi_{\min} = 0.1$.)

Conclusions

The damage model for brittle materials developed by Grinfeld was installed into LS-DYNA. This model introduces a damage state variable D . The model consists of an evolution equation for D and a degradation function of D . The degradation function is applied multiplicatively to the elastic shear modulus of an isotropic linearly elastic material; Poisson's ratio is unaltered.

The model was applied to simulations of normal plate-on-plate impact. We scaled the initial-value, boundary-value problem and found the occurrence of only two dimensionless parameters, ϕ_{\min} and Π . The latter is a combination of pre-damaged elastic properties, material properties introduced by the damage model, target geometry, and impact speed. The LS-DYNA solutions for various Π were examined with regard to the failure wave hypothesis sketched in Figure 1b. For $\Pi = 0.1$ and 0.2 , the normal velocity of the target's free surface was seen to gradually increase slightly from its level associated with the initial arrival of the compressive shock. For $\Pi = 0.3$ and 0.4 , the free-surface velocity was seen to gradually decrease from its level associated with the initial arrival of the compressive shock. The solutions for damage and stress fields within the target revealed two competing mechanisms. The evolution of damage led to stiffness gradients within the target, which did indeed produce gradual reflections of the unloading wave back to the free surface. However, damage evolution also led to a reduction of the compressive stress field, which acted to reduce the free-surface velocity.

A proposed change to the Grinfeld model that may lead to the distinct recompression plateau in Figure 1b is to replace the linear $\phi(D)$ relationship of equation 7. A more abrupt change of ϕ with D may achieve both goals of a more abrupt reflection of the loading wave and a smaller degradation in the stress amplitude of the unloading wave prior to encountering the abrupt change in ϕ .

Since the evolution equation is based on elastic strain energy, a quadratic function of the strain components, the damage model does not distinguish damage contributions from tension and compression. This issue can also be addressed in a future refinement.

References

1. Kanel GI, Rasorenov SV, Fortov VE. The failure waves and spallations in homogeneous brittle materials. In: Schmidt SC, Dick RD, Forbes JW, Tasker DG, editors. Shock Compression of Condensed Matter – 1991: Amsterdam: North-Holland, 1992. p. 451–454.
2. Brar NS, Bless SJ. Failure waves in glass under dynamic compression. High Pressure Research 1992; 10: 773–784.
3. Grinfeld MA, Wright TW. Thermodynamics of brittle fracture. U.S. Army Research Lab. Report ARL-TR-3659, 2005.
4. Grinfeld MA, Wright TW, Schoenfeld SE. Failure fronts in brittle materials and their morphological instabilities. In: Furnish MD, Elert ML, Russell TP, White CT, editors. Shock Compression of Condensed Matter – 2005: Amsterdam: North-Holland, in press.
5. Livermore Software Technology Corporation. LS-DYNA Keyword User's Manual. Version 970, Livermore, CA, 2003.
6. Coleman BD, Gurtin ME. Thermodynamics with internal state variables. The Journal of Chemical Physics 1967; 47: 597–613.

